Available online at www.sciencedirect.com
SCIENCE DIRECT®
Control Engineering Practice 14 (2006) 121–136
CONTROL ENGINEERING PRACTICE
www.elsevier.com/locate/conengprac

Adaptive control of automotive electronic throttle

Danijel Pavković[a,*], Joško Deur[a], Martin Jansz[b], Nedjeljko Perić[c]

[a]Faculty of Mechanical Engineering and Naval Architecture, University of Zagreb, I. Lučića 5, HR-10000 Zagreb, Croatia
[b]Ford Motor Company Ltd., Product Development Europe, Dunton Technical Centre, Laindon, Basildon, Essex SS15 6EE, UK
[c]Faculty of Electrical Engineering and Computing, University of Zagreb, Unska 3, HR-10000, Zagreb, Croatia

Received 16 June 2003; accepted 19 January 2005
Available online 3 March 2005

Abstract

An electronic throttle is a DC servo drive which positions the throttle plate, thus providing drive-by-wire control of engine torque. This paper presents an electronic throttle control strategy consisting of a PID controller, and nonlinear friction and limp-home compensators. The emphasis is on the development of an adaptive control strategy, which is aimed to enhance the control strategy robustness with respect to process parameter variations, caused by production deviations, variations of external conditions, and aging. The adaptive strategy consists of auto-tuning and self-tuning algorithms. The auto-tuner provides automatic tuning of the control strategy parameters during vehicle assembly, or uses specific drive modes during normal use (e.g. each time the engine is turned off). The self-tuning algorithms are based on the permanent, on-line estimation of those process parameters which can vary within a single engine run (e.g. the DC motor armature resistance). The presented adaptive control strategy has been verified experimentally.

Keywords: Servomotors; Automotive control; Electric throttle control; Friction; Nonlinear control; Auto-tuner; Self-tuning control

1. Introduction

In conventional vehicles the driver gas pedal is mechanically linked to the throttle plate. This system is being replaced in modern vehicles by an electronic throttle, where the link between the gas pedal and the throttle plate is realized by means of a DC servomotor. In this way, the engine control unit can correct the throttle position reference value for specific engine operating modes, thus improving drivability, fuel economy, and emissions, and also providing the implementation of engine-based vehicle dynamics control systems including traction control (Huber, Liebenroth-Leden, Maisch, & Reppich, 1991). The electronic throttle consists of an electronic throttle body, a chopper, and a position control strategy. A photograph of an electronic throttle body is shown in Fig. 1a, and its internal structure is depicted in the lower right part of Fig. 1b. The electronic throttle servo system does not usually include an inner current controller. The throttle motion is constrained by a dual return spring which returns the throttle in the so-called limp-home (LH) position in the case of power supply failure.

It has been demonstrated in (Deur, Pavković, Perić, Jansz, & Hrovat, 2004) that DC drive transmission friction and the dual return spring nonlinearity at the LH position significantly affect the performance of the electronic throttle control system. A nonlinear control strategy is proposed in the same reference in order to compensate for friction and LH nonlinear effects, thus providing a linear system-like behavior for a wide range of throttle operation. The step response of control system is characterized by the settling time of approximately 70 ms and the steady-state accuracy better than 0.1°. The control strategy has been tuned based on the

*Corresponding author. Tel.: +385 1 6168325; fax: +385 1 6168351.
E-mail addresses: danijel.pavkovic@fsb.hr (D. Pavković), josko.deur@fsb.hr (J. Deur), mjansz@ford.com (M. Jansz), nedjeljko.peric@fer.hr (N. Perić).

0967-0661/$ - see front matter © 2005 Elsevier Ltd. All rights reserved.
doi:10.1016/j.conengprac.2005.01.006

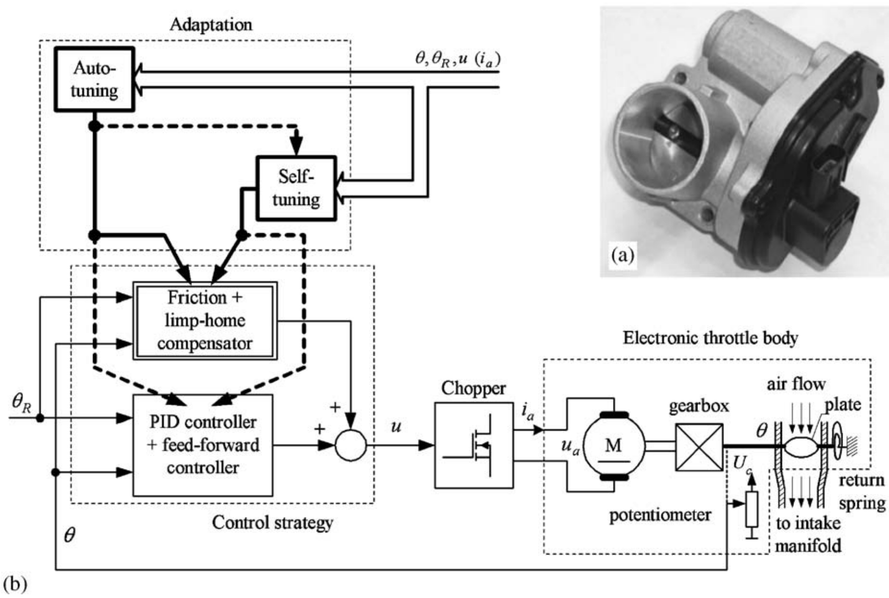

Fig. 1. Photograph of electronic throttle body (a), and principal schematic of adaptive electronic throttle control system (b).

results of off-line experimental identification of electronic throttle process model (see Pavković, Deur, Jansz, & Perić, 2003).

It can be expected that the performance of an electronic throttle with constant controller parameters will deteriorate in the presence of process parameter variations. There are three sources of process parameter variations (see Pavković & Deur, 2002; Hashimoto, Ishiguro, Yasui, & Akazaki, 2003):

(a) *Production deviations.* Different ETBs from the same production series can have different parameters. Static curves $u(\theta)$ in Fig. 2a illustrate that the friction level characterized by the width of the static curve hysteresis, and the LH voltage step can be quite different for different ETBs.
(b) *Aging.* Fig. 2b indicates that the friction and LH voltages increase with aging of ETB. The LH position has been found to vary with aging as well. Aging may also decrease the DC motor voltage and torque constants due to the weakening of the motor permanent magnets.
(c) *Variations of external temperature and battery voltage.* The DC motor armature resistance can vary in the range 1:2 as the consequence of temperature variations (Hashimoto et al., 2003). This has direct implications on the friction and LH voltage parameters, as illustrated by the static curves in Fig. 3. The battery voltage variations have similar influence on the process static curve parameters.

In order to deal with process parameter variations, two control concepts can generally be applied: (i) robust control and (ii) adaptive control. The former concept assumes that the process model uncertainties can be captured by means of a specific control structure. A sliding mode electronic throttle control structure is often proposed either in its standard form (see e.g. Hashimoto et al., 2003; Rossi, Tilli, & Tonielli, 2000; Yokoyama, Shimizu, & Okamoto, 1998) or in a more advanced neural network-based form (see e.g. Barić, Petrović, & Perić, 2002, 2004). The effectiveness of such an approach can be limited by high level of noise in the controller output signal (chattering), and/or the requirements on very low sampling time and powerful processor. The latter concept of adaptive control assumes on-line tuning of controller parameters based on the results of on-line process identification. Such a concept has not been well investigated in the available literature, with an exception of Hashimoto et al. (2003), and Gagner and Bondesson (2000), where adaptive LH compensators are presented.

This paper proposes a more comprehensive adaptive electronic throttle control strategy compared to those given in Hashimoto et al. (2003), and Gagner and Bondesson (2000), and presents the results of thorough experimental tests. The adaptation mechanism tunes the control strategy from Deur et al. (2004) with respect to wide-range variations of all process parameters. The overall adaptive control strategy can be implemented on a low-cost automotive microcontroller system with integer arithmetic only and typical electronic throttle sampling time in the range from 2 to 5 ms. The adaptation strategy consists of auto-tuning and self-tuning algorithms (Fig. 1b).

The auto-tuner tunes the controller parameters for each single ETB in the stage of vehicle production. It can also be executed during specific vehicle drive modes

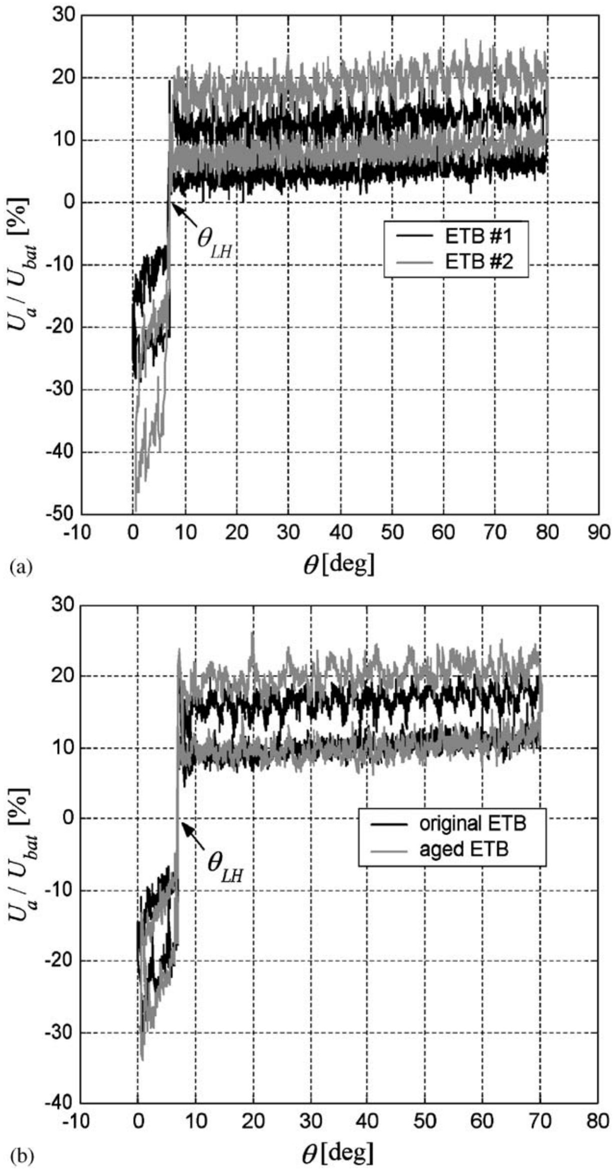

Fig. 2. Variations of process static curves for different ETBs (a), and variations of process static curve parameters due to aging (b).

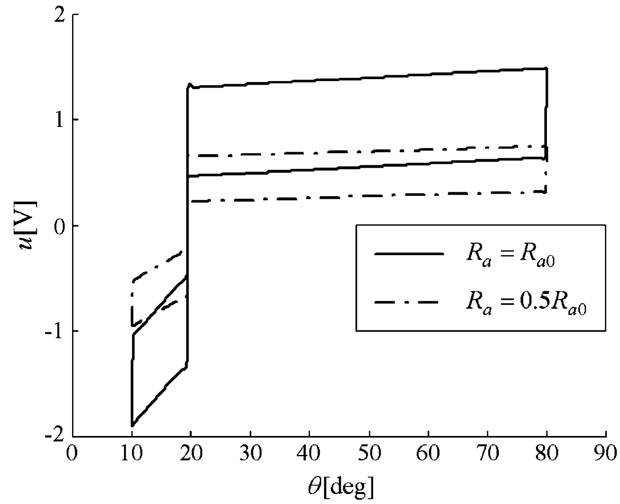

Fig 3. Influence of armature resistance on process static curve (simulation).

(e.g. during maintenance intervals, or each time the engine is turned off), thus adapting the control strategy with respect to slow variations of process parameters (e.g. friction and LH variations). The self-tuning algorithm performs real-time estimation of those process parameters which can vary within a single engine run (e.g. armature resistance), and updates the relevant control strategy parameters.

The paper is organized in seven sections. Section 2 describes the process model. Section 3 presents the nonlinear control strategy, and gives some illustrative experimental results. A simulation analysis of the influence of process parameter variations on the electronic throttle performance is presented in Section 4. The auto-tuner is described in Section 5. Section 6 presents self-tuning algorithms which adapt the control strategy with respect to variations of armature resistance, battery voltage, and LH position. Different variants of armature resistance estimator are proposed, depending on the availability of armature current measurement and auto-tuning procedure. Both auto-tuning and self-tuning algorithms are verified experimentally. Concluding remarks are given in Section 7.

2. Process model

The process model is shown in Fig. 4 (see e.g. Scattolini et al., 1997). The high-bandwidth dynamics of the chopper is approximated by the proportional term with the gain K_{ch}. The electronic throttle body is described by the well-known DC motor linear model which is extended with nonlinear models of friction and dual return spring. A dynamic friction model is used in simulations. It represents an extension of the Dahl friction model, and is described in detail in Deur et al. (2004). The load torque m_L due to the throttle air mass flow has not been found to have significant influence on the electronic throttle behavior, and it is treated as an unknown disturbance.

Fig. 5 shows the process static curve (cf. Fig. 2). The voltage parameters of the process static curve are related to the corresponding LH and friction torques as follows (cf. Figs. 4 and 5):

$$2U_{LH} = \frac{K_l \Delta M_{LH}}{K_{ch} K_a K_t}, \tag{1}$$

$$U_{S,C} = \frac{M_{S,C}}{K_{ch} K_a K_t}. \tag{2}$$

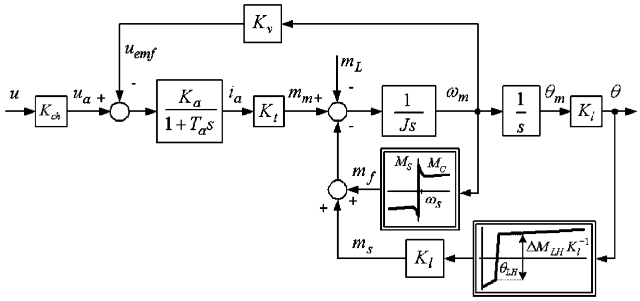

Fig. 4. Block diagram of electronic throttle process. u, u_a, u_{emf} - commanded signal, armature voltage, and back electromotive force; i_a - armature current; m_m, m_s, m_f, m_L - motor, return spring, friction, and load torque; θ_m, θ - motor and throttle position; ω_m - motor speed; K_{ch} - chopper gain; K_a, K_t, K_v - armature, torque, and voltage gain; J - total moment of inertia; $1/K_l$ - gear ratio; θ_{LH} - limp-home position; M_C, M_S - Coulomb and breakaway friction.

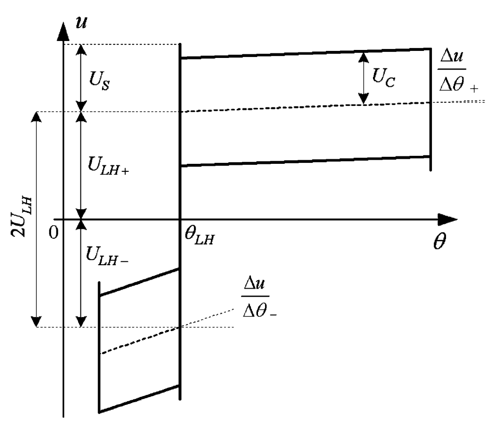

Fig. 5. Process static curve.

In general, the values of LH voltages $U_{LH\pm}$ and the slopes of process static curve $\Delta u/\Delta\theta_{\pm}$ above$_{(+)}$ and below$_{(-)}$ the LH position θ_{LH} are not equal.

According to Pavković et al. (2003), the armature time constant is very small ($T_a \approx 0.5\,\text{ms}$), and it does not affect the linear process dynamics. Thus, the linear process model (Fig. 4 with $m_f = 0$ and $m_s = K_s K_l \theta$) can be described by the second-order lag model:

$$G_p(s) = \frac{\theta(s)}{u(s)} = \frac{K_{p2}}{1 + a_{p1}s + a_{p2}s^2}, \tag{3}$$

with

$$K_{p2} = \frac{K_{ch}K_aK_t}{K_sK_l}, \quad a_{p1} = \frac{K_d}{K_sK_l^2}, \quad a_{p2} = \frac{J}{K_sK_l^2}, \tag{4}$$

where K_d is the damping coefficient due to the back electromotive force u_{emf}:

$$K_d = K_aK_tK_v. \tag{5}$$

If the return spring stiffness K_s is small enough (i.e. if the slope of the process static curve is small), so that the following condition is satisfied:

$$K_d \gg K_l\sqrt{2K_sJ}, \tag{6}$$

the linear process dynamics can be represented by a simple integral + lag model (IT_1 model) (see Deur et al., 2004):

$$G_p(s) = \frac{\theta(s)}{u(s)} = \frac{K_p}{s(1 + T_{em}s)}, \tag{7}$$

where the process gain K_p and the electromechanical time constant T_{em} are given by

$$K_p = K_{ch}K_l/K_v,$$
$$T_{em} = J/K_d. \tag{8}$$

According to identification results in Pavković et al. (2003), the condition (6) is satisfied in the region above the limp home position ($\theta > \theta_{LH}$, cf. slopes of the process static curve in Fig. 2 for $\theta < \theta_{LH}$ and $\theta > \theta_{LH}$).

3. Nonlinear control strategy

Fig. 6 shows the block diagram of the proposed electronic throttle control strategy. The control strategy consists of a PID feedback controller, a first-order lead-lag feedforward controller (FFC), and nonlinear friction and LH compensators. Brief description of the control strategy structure, tuning, and experimental verification is given in the next subsections. More detailed elaboration can be found in Deur et al. (2004).

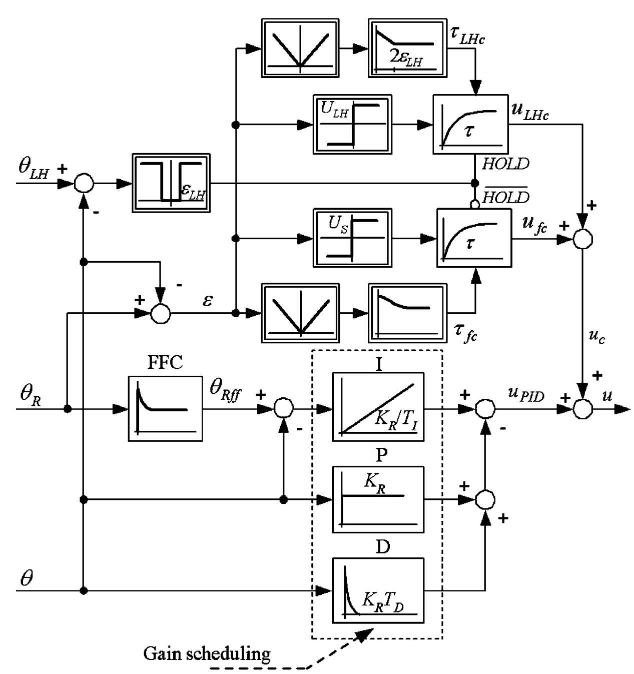

Fig. 6. Electronic throttle control strategy.

3.1. PID controller and feedforward controller

Design of the linear control system with discrete-time PID controller is carried out in the continuous-time domain. The sampler and the zero-order-hold element, as well as the time-differentiator used in the controller derivative term, are approximated by a parasitic first-order lag term with the time constant $T \ll T_{em}$ (T—sampling time). The basic set of PID controller parameters (for the region $\theta > \theta_{LH}$) is calculated based on the parameters K_p and T_{em} of the IT_1 process model given by Eq. (7). The controller parameters are optimized according to the damping optimum analytical design method (see Naslin, 1968; Zäh & Brandenburg, 1987; Deur, 2001). Calculating the closed-loop system characteristic polynomial, and equating it with the third-order damping optimum characteristic polynomial:

$$A(s) = D_2^3 D_3 T_e^3 s^3 + D_2 T_e^2 s^2 + T_e s + 1 \tag{9}$$

yields the following simple equations for the controller parameters:

$$K_{R+} = \frac{1}{K_p} \frac{T_{em} + T}{D_2^2 D_3 T_e^2}, \tag{10}$$

$$T_{D+} = D_2 T_e \left(1 - \frac{D_2 D_3 T_e}{T_{em} + T}\right), \tag{11}$$

$$T_{I+} = T_e. \tag{12}$$

By setting the characteristic ratios D_2 and D_3 to the optimal value 0.5, the resulting closed-loop system is characterized by the quasi-aperiodic step response with the overshoot of 6% and the rise time of $1.8T_e$, and correspondingly with the gain margin, phase margin and critical frequency of 10 dB, 60° and $2.9/T_e$, respectively. The characteristic ratios D_2 and D_3 are decreased here below the optimal value 0.5 ($D_2 = 0.37$ and $D_3 = 0.4$), in order to provide the boundary aperiodic step response of the control system. The equivalent time constant of the closed-loop system T_e determines the response time, and can be chosen arbitrarily to a value larger than

$$T_{e,\min} = \frac{2}{D_2 D_3} \frac{T}{1 + T/T_{em}}. \tag{13}$$

Since the return spring is significantly stiffer in the region $\theta < \theta_{LH}$ than in the region $\theta > \theta_{LH}$ (Fig. 2), the control system tuned according to Eqs. (10)–(12) would have slower response in the region $\theta < \theta_{LH}$. In order to provide the same control performance for both regions, the return spring influence must be taken into account, i.e. a second-order lag process model (3) must be used instead of the IT_1 model (7). The final equations for the optimal controller parameters for $\theta < \theta_{LH}$ can conveniently be expressed as exact modifications of the basic expressions (10)–(12):

$$K_{R-} = K_{R+} - \frac{\Delta u}{\Delta \theta_-}, \tag{14}$$

$$T_{I-} = T_{I+}\left(1 - \frac{D_2^2 D_3 T_e^2}{T_{em} + T} K_p \frac{\Delta u}{\Delta \theta_-}\right), \tag{15}$$

$$T_{D-} = T + (T_{D+} - T)\left(1 - \frac{D_2^2 D_3 T_e^2}{T_{em} + T} K_p \frac{\Delta u}{\Delta \theta_-}\right)^{-1}, \tag{16}$$

where $\Delta u / \Delta \theta_-$ is defined in Fig. 5. The change of PID controller parameters with respect to operating region ($\theta < \theta_{LH}$ or $\theta > \theta_{LH}$) is achieved by applying a simple gain-scheduling algorithm with bump-less transfer included.

The feedforward controller introduces a discrete-time zero z_{ff} into the overall closed-loop transfer function, thus speeding up the response with respect to the reference signal. The zero is determined based on the zero-pole canceling approach:

$$z_{ff} = \exp(-2T/T_e). \tag{17}$$

3.2. Friction and LH compensation

The PID controller can provide favorable electronic throttle behavior in the large-signal operating mode (for large changes of reference position θ_R). However, the electronic throttle performance significantly deteriorates in the small-signal operating mode due to the friction and LH nonlinear effects. The experimental results in Fig. 7a point out to unacceptable slow control system response with respect to reference step change of 0.2°. The slow response is a consequence of the stiction influence. Similarly, a significant response delay (a standstill interval) appears while the throttle passes through the nonlinear LH region (Fig. 8).

In order to improve the control system performance in the small-signal operating mode, the PID controller is extended with friction and LH compensators with outputs u_{fc} and u_{LHc}, respectively (Fig. 6). The compensators have the same structure, because the friction and LH nonlinearities have similar relay-type static curves and similar influences to the control system behavior (Fig. 4). Only one of the two compensators is active at any time, depending on whether the throttle is inside or outside the LH region. The LH compensator threshold parameter ε_{LH} is typically set to the double value of position measurement resolution $\Delta_\theta \approx 0.1°$.

The compensators act as bang–bang feedback controllers. Thus, they tend to provide fast and robust elimination of the control error ε. The magnitudes of the friction and LH bang–bang controllers, U_{LHc} and U_{Sc}, are set near the values of the LH and friction

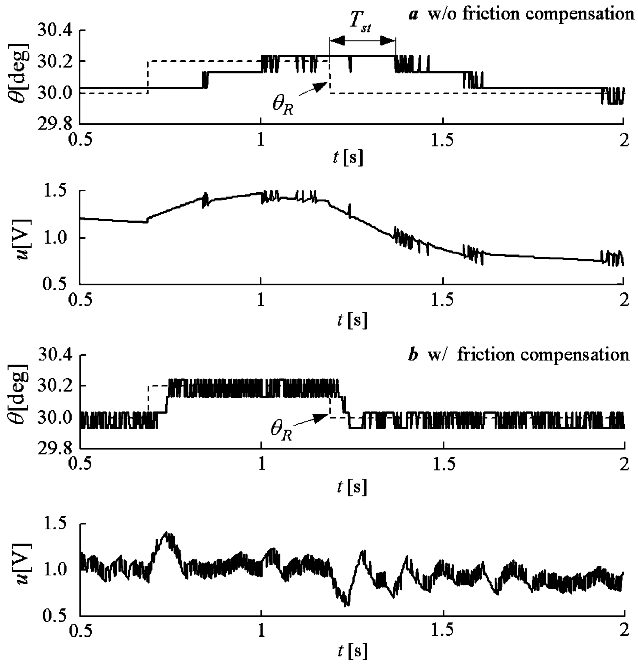

Fig. 7. Experimental step responses of systems without (a) and with friction compensator (b).

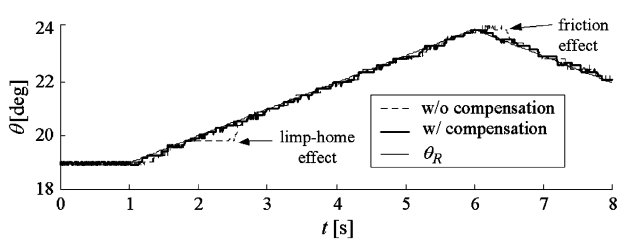

Fig. 8. Experimental ramp tracking responses of systems without and with friction and LH compensator.

voltages U_{LH} and U_S:

$$
\begin{aligned}
&U_{LHc} = \kappa_{LH} U_{LH},\\
&U_{Sc} = \kappa_S U_S,\\
&\kappa_{LH}, \kappa_S \approx 1.
\end{aligned}
\tag{18}
$$

Therefore, the compensator action is limited to the critical nonlinear small-signal operating mode only, without disturbing (destabilizing) the control system in the large-signal operating mode. Namely, the overall control strategy can be regarded as a dual controller, where the PID controller dominantly determines the closed-loop system behavior in the large-signal operating mode, and the nonlinear compensators are responsible for the small-signal operating mode.

The main problem with the use of bang–bang controller is a large level of noise in the commanded signal u (the chattering effect), which can cause transmission and potentiometer wear, and excessive motor losses. In order to avoid the chattering effect, a unit-gain first-order low-pass filter is cascaded to the bang–bang controller (Fig. 6). In the case of friction compensation, the filter use is also beneficial from the standpoint of avoiding the step response overshoots due to the stiction dynamics. The filter time constants τ_{fc} and τ_{LHc} may be made dependent on the absolute value of the control error ε to obtain the best performance (see Deur et al., 2004 for explanation of tuning the lookup table $\tau_{fc}(|\varepsilon|)$). It has been found, however, that even constant values $\tau_{fc} \approx 70$ ms and $\tau_{LHc} \approx 15$ ms give good results for the particular electronic throttle.

The step responses in Fig. 7 and ramp responses in Fig. 8 indicate that the friction and LH compensation results in significant reduction of stiction and LH standstill intervals, thus making the responses similar to those of the linear system. Also, the important benefit of friction compensation is fast establishing the one-bit limit-cycle steady-state response (Fig. 7). Such a behavior is desirable in order to decrease the control error even below the position measurement resolution (0.1° here). It is important to note that the above benefits are reached without any significant increase of the noise magnitude in the commanded signal u (cf. Fig. 7a and b). More detailed results of experimental verification of the control strategy are included in Deur et al. (2004), and Pavković (2003).

4. Influence of process parameter variations

4.1. Armature resistance variations

The variations of armature resistance $R_a = K_a^{-1}$ affect both the parameters of linear and nonlinear parts of the control system (Eqs. (1)–(5)). It is reasonable to assume that the armature resistance variations do not exceed $\pm 50\%$ of the nominal value R_{a0} ($R_a \in [0.5R_{a0}, 1.5R_{a0}]$).

4.1.1. Linear control system

The linear control system consists of the PID controller and the linear process model given in Fig. 4, with $m_f = 0$ and $m_s = K_l K_s \theta$. Fig. 9 shows simulation step responses of the linear control system for different values of armature resistance. These step responses point out to small sensitivity of the linear control system to armature resistance variations. This result has been proven analytically by Pavković and Deur (2002). The linear control system sensitivity is somewhat larger in the presence of feedforward controller (Pavković, 2003).

4.1.2. Nonlinear control system

The overall nonlinear control system is affected by the armature resistance change through the change of the breakaway voltage U_S and the LH voltage U_{LH}

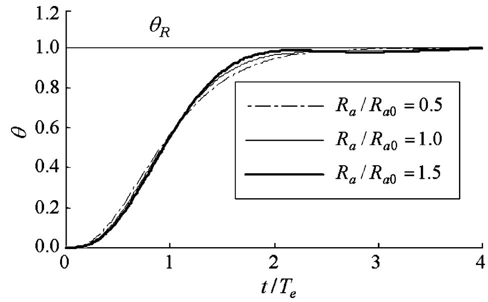

Fig. 9. Unit step responses of linear control system without feedforward controller for different values of armature resistance.

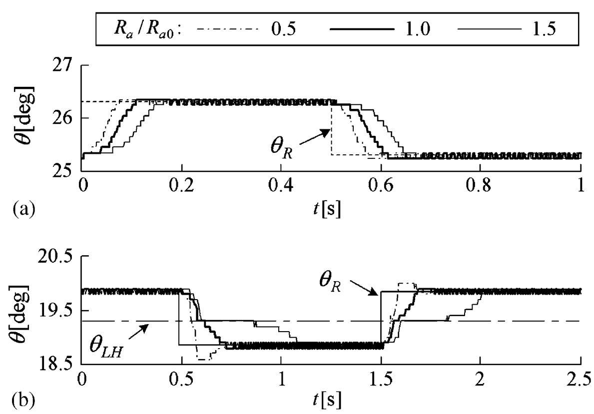

Fig. 10. Influence of armature resistance variations on performance of friction compensation (a) and LH compensation (b).

(Figs. 5 and 3):

$$U_{LH} = U_{LH0}\frac{K_{a0}}{K_a} = U_{LH0}\frac{R_a}{R_{a0}}, \tag{19}$$

$$U_S = U_{S0}\frac{K_{a0}}{K_a} = U_{S0}\frac{R_a}{R_{a0}}. \tag{20}$$

The non-adaptive control system with constant parameters $U_{Sc} = \kappa_S U_{S0}$ and $U_{LHc} = \kappa_{LH} U_{LH0}$, and variable process parameters U_S and U_{LH} will obviously have sub-optimal behavior if $R_a \neq R_{a0}$.

This is confirmed by the simulation step responses shown in Fig. 10. The step responses show that overcompensation of nonlinear effects occurs for $R_a < R_{a0}$ (the step response is faster with possible occurrence of an overshoot), while undercompensation of nonlinear effects occurs for $R_a > R_{a0}$ (significant standstill interval can be observed). The LH compensator is more sensitive to armature resistance variations than the friction compensator, primarily because $U_{LH} > U_S$.

4.2. Battery voltage variations

The chopper gain K_{ch} is proportional to the battery voltage U_{bat} (Pavković et al., 2003). In the low-speed nonlinear operating region ($u_{emf} \approx 0$), the chopper gain K_{ch} is cascaded to the armature gain $K_a = 1/R_a$ (Fig. 4). Thus the influence of the battery voltage variations is the same in this operating mode as the influence of armature resistance variations (Section 4.1).

The response in the large-signal operating mode is expected to be more sensitive to the battery voltage variations than to variations of armature resistance, because the gain K_{ch} appears outside the u_{emf} damping path (Fig. 4). However, the battery voltage varies in a narrower range (typically $\pm 20\%$ of the nominal battery voltage U_{bat0}, compared with $\pm 50\%$ armature resistance variations. Thus, the influence of battery voltage variations to the control system response in the large-signal operating mode is not emphasized either, as illustrated by simulation results in (Pavković & Deur, 2002).

4.3. Variations of LH position

The LH compensator is only active in a narrow region around the supposed LH position $\theta_{LH0} \pm \varepsilon_{LH}$ (Fig. 6). If the information θ_{LH0} about the LH position were inaccurate, the LH compensator would be activated outside the actual LH position θ_{LH}. This can cause undesirable behavior of the electronic throttle control system.

The influence of inaccurate LH position θ_{LH} is illustrated by simulation step responses in Fig. 11. The simulation responses are compared with the first-order reference model response θ_m, which describes the desired behavior of the linear part of the electronic throttle control system. In the case when the actual limp home position θ_{LH} is within the LH threshold ($|\theta_{LH} - \theta_{LH0}| \leqslant \varepsilon_{LH}$), the throttle position response θ is close to the model response θ_m, i.e. the LH standstill interval is relatively small and there is no overshoot in control system response. However, when the actual LH position exceeds the LH compensator threshold ($|\theta_{LH} - \theta_{LH0}| > \varepsilon_{LH}$), a large discrepancy between the model response and the real response is observed, particularly at the actual LH position where the throttle is stuck for a considerable time. An undesirable overshoot can also

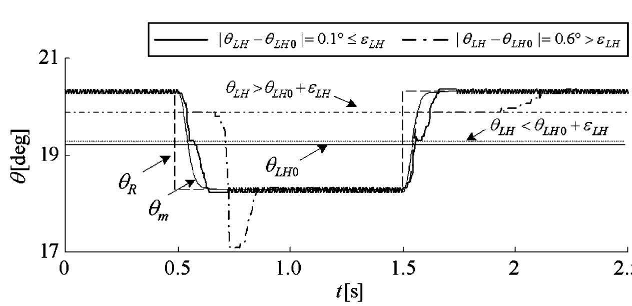

Fig. 11. Influence of LH position variations.

occur due to the inappropriate action of the LH compensator (Fig. 11).

5. Automatic tuning of control strategy

The electronic throttle control strategy in Section 3 is extended with an automatic tuning (auto-tuning) procedure, in order to deal with slow variations of process parameters.

5.1. Auto-tuner outline

The schematic in Fig. 12 outlines how the auto-tuner works. There are six characteristic phases of auto-tuner operation, which are denoted in Fig. 12 by encircled numbers and arrows. Each phase relates to either a single point or a portion of the process static curve, and can be executed in open loop (ol) or closed loop (cl). Fig. 12 also shows which type of the commanded signal u or the reference signal θ_R is applied in each phase.

The auto-tuner determines the LH position θ_{LH} in the initial phase 0 when $u = 0$ is set. In phase 1 the throttle is positioned to the upper edge of the static curve at $\theta = \theta_{LH}$, i.e. to the left most operating point of the approximately linear operating region $\theta > \theta_{LH} \wedge \dot{\theta} > 0$ of the static curve (the nonlinear friction and LH influences are overcome). At the beginning of phase 2, a step change of the commanded signal u is applied. Based on the throttle position response the parameters of dominant linear process dynamics are estimated. Using the estimated process parameters, the basic set of PID controller parameters (for $\theta > \theta_{LH}$) is determined at the beginning of phase 3. The throttle is then brought (under the PID control) to the position θ_0, which is somewhat larger than the LH position θ_{LH}. In phase 4, the ramp change of the throttle position reference θ_R through the static curve region $\theta < \theta_0$ is commanded. In this way, the main parameters of the process static curve are estimated. Based on these estimates, final tuning of the control strategy is carried out in phase 5.

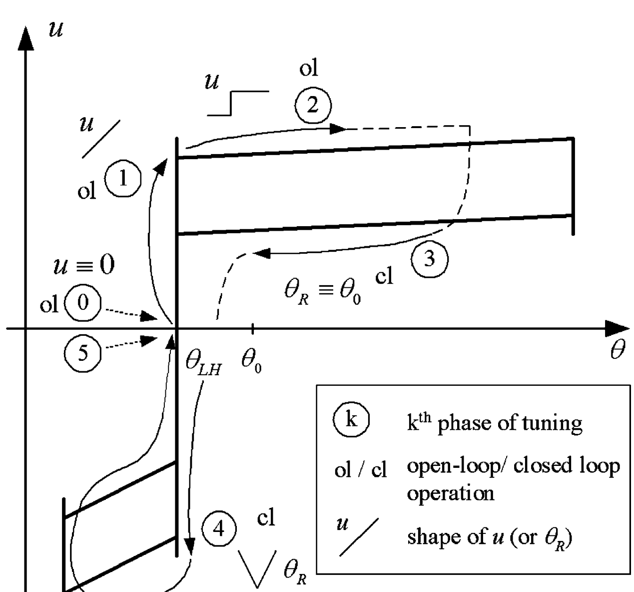

Fig. 12. Illustration of auto-tuning operations.

5.2. Process identification

The auto-tuning operation during the identification phases 0, 1, 2, and 4 is described. The description is illustrated by the experimental response shown in Fig. 13. The overall auto-tuning procedure lasts about 1.5 s.

5.2.1. Phase 0—LH position estimation

The LH position θ_{LH} is simply determined as the average throttle position during the first several instants of auto-tuner execution (when $u \equiv 0$).

5.2.2. Phase 1—Breakaway from LH position

The main task of the auto-tuner during phase 1 is to bring the throttle to the upper point of the LH region (Fig. 12). This needs to be done in a relatively short period, using the open-loop control only, and having no prior knowledge of the process static curve parameters. Phase 1 is divided in two stages. In the first stage, the commanded signal u is ramped-up until the breakaway

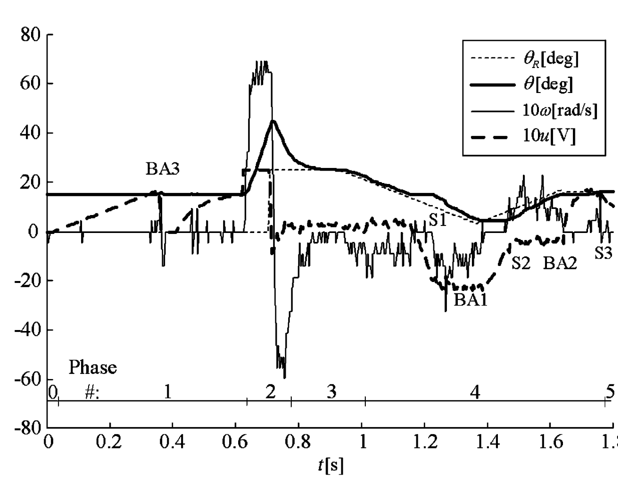

Fig. 13. Experimental responses of electronic throttle during auto-tuning procedure.

from the LH position is detected (the interval $t = 0$–$0.35\,\mathrm{s}$ in Fig. 13). The reached commanded signal u is saved as the breakaway voltage u_{ba}. In order to avoid slow throttle transition through the region $\theta > \theta_{LH}$ and possible excess of the upper stop position, the throttle is returned to the LH position in the second stage by setting $u = 0$. It is then quickly brought close to the breakaway operating point u_{ba} (but without breakaway) by applying an exponential form of the commanded signal u (the interval 0.35–0.65 s in Fig. 13).

There are two practical aspects of auto-tuner implementation for phase 1 (Deur & Pavković, 2002): (i) choice of the rate of change of the commanded signal u during the first stage, and (ii) breakaway detection. The u-rate is chosen to a maximum value that still provides an accurate estimation of u_{ba}. The breakaway instant k_{ba} is found as the first sampling instant after which the sum of three consecutive throttle speed samples is greater or equal to $5\Delta_\omega$ ($\Delta_\omega = \Delta_\theta / T$ is the speed measurement quantization level), i.e. when $\omega(k_s+1) + \omega(k_s+2) + \omega(k_s+3) \geqslant 5\Delta_\omega$. Using the throttle speed reconstruction equation $\omega(k) = [\theta(k) - \theta(k-1)]/T$ yields the breakaway condition

$$\theta(k_s+3) - \theta(k_s) \geqslant 5\Delta_\theta. \tag{21}$$

The breakaway voltage is given by

$$u_{ba} = u(k_{ba}), \quad k_{ba} = \min\{k_s\}. \tag{22}$$

5.2.3. Phase 2—Identification of linear process dynamics

According to the analysis in Section 2, the linear process model may be approximated in the region $\theta > \theta_{LH}$ by (cf. Eq. (7)):

$$G_{p\omega}(s) = \frac{\omega(s)}{u(s)} = s\,\frac{\theta(s)}{u(s)} = \frac{K_p}{1 + T_{em}s}. \tag{23}$$

Hence, the throttle speed step response can simply be described as

$$\omega(t) = \omega_{ss}(1 - \mathrm{e}^{-t/T_{em}}). \tag{24}$$

The throttle speed response in Fig. 13 (phase 2) is indeed in agreement with the description (23). The process gain K_p is estimated as $K_p = \omega_{ss}/\Delta u$, where ω_{ss} is the speed response steady-state value, and Δu is the commanded signal step change. In order to avoid time-consuming numerical optimization of T_{em} (applied by Pavković et al., 2003 for off-line process identification), it is convenient to integrate the speed response and find a relation between the speed integral (i.e. the displacement $\theta_{fin} - \theta_{init}$) and T_{em}:

$$\begin{aligned} \int_0^{T_{fin}} \omega \mathrm{d}t &= \theta_{fin} - \theta_{init} \\ &= \omega_{ss} \int_0^{T_{fin}} (1 - \mathrm{e}^{-t/T_{em}}) \mathrm{d}t \\ &= \omega_{ss}[T_{fin} - T_{em}(1 - \mathrm{e}^{-T_{fin}/T_{em}})]. \end{aligned} \tag{25}$$

Since the identification interval T_{fin} is larger than $3T_{em}$ (the steady-state condition), the exponential term on the rightmost side of Eq. (25) is less then 0.05 and may be neglected. Hence,

$$T_{em} \approx T_{fin} - \frac{\theta_{fin} - \theta_{init}}{\omega_{ss}}. \tag{26}$$

In order to calculate the steady-state speed ω_{ss} and determine T_{fin}, it is necessary to detect the steady-state portion of the speed response. The steady-state instant k_{ss} is determined as the first sampling instant after which the absolute value of the sum of N consecutive throttle speed differences is less than or equal to the speed quantization level Δ_ω, i.e.

$$k_{ss} = \min\{k_r\}, \tag{27}$$

where k_r satisfies the relation

$$\left| \sum_{i=1}^{N} \omega(k_r+i) - \omega(k_r+i-1) \right| \leqslant \Delta_\omega. \tag{28}$$

The final throttle position θ_{fin} and the steady-state speed ω_{ss} are then determined as

$$\theta_{fin} = \theta(k_{ss}), \tag{29}$$

$$\omega_{ss} = \frac{1}{N_1 + M} \sum_{i=N-N_1+1}^{N+M} \omega(k_{ss}+i), \tag{30}$$

where $N_1 < N$ is the number of last several samples inside the sampling window used in Eq. (28), and M, is the number of additional subsequent samples. Typical values of these constants are $N = 5$, $N_1 = 3$, $M = 7$.

5.2.4. Phase 4—Identification of process static curve

The required process static curve parameters U_S, U_{LH}, and $\Delta u/\Delta\theta_-$ (Fig. 5) can be reconstructed from the relatively narrow portion of the overall static curve around the region $\theta \leqslant \theta_0$ in Fig. 12. The static curve is recorded as the closed-loop response with respect to ramp form of the position reference θ_R. The ramp slope is set to a maximum value that still provides a reasonably accurate prediction of the static curve. The recorded static curve is shown in Fig. 14 (solid line).

Estimation of the static curve parameters by Pavković et al., 2003 was based on off-line straight-line interpolations of the static curve. This technique is not suitable for on-line estimation, because of the high computational requirements and certain inaccuracy of the on-line recorded static curve (cf. static curves in Fig. 14). Therefore, another identification method based on the characteristic points of the static curve is proposed. There are six characteristic points (Fig. 14), which can be divided in two characteristic groups: the breakaway points BA1-BA3, and the sliding-regime points S1-S3. The breakaway point BA3 was already identified in

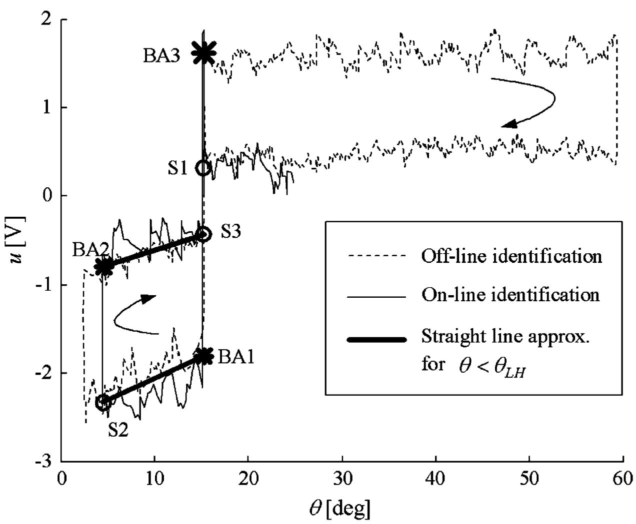

Fig. 14. Process static curves recorded by off-line and on-line experiments, and results of on-line identification, denoted by '*' and 'o' symbols.

phase 1 ($u_{BA3} = u_{ba}$), and the other two breakaway points BA1 and BA2 are identified in the similar way (see Deur & Pavković, 2002). The voltage levels of the sliding-regime points S_j, $j = 1, 2, 3$ are estimated by averaging the commanded signal u over a narrow sliding interval:

$$u_{Sj} = \frac{1}{L}\sum_{i=1}^{L} u(k_{Sj} + i), \tag{31}$$

where L is typically 5–8 samples.

Averaging starts at the sampling instant k_{Sj} which is determined based on the following conditions (Fig. 12):

$$\begin{aligned} &\theta_R(k_{Sj}) < \theta_{LH} \quad \text{for } j = 1,\\ &\theta_R(k_{Sj}) > \theta_R(k_{Sj} - 1) \quad \text{for } j = 2,\\ &\theta_R(k_{Sj}) > \theta_{LH} \wedge u_{BA2} \quad \text{already estimated for } j = 3. \end{aligned} \tag{32}$$

Once the characteristic voltage levels u_{BAi} and u_{Si} are estimated (see * and o-marks in Fig. 14), the required static curve parameters U_S, U_{LH}, and $\Delta u/\Delta\theta_-$ (Fig. 5) are readily calculated as

$$U_S = \frac{1}{2}\left[\frac{u_{BA3} - u_{S1}}{2} + \frac{1}{2}\left(\frac{u_{S3} - u_{BA1}}{2} + \frac{u_{BA2} - u_{S2}}{2}\right)\right], \tag{33}$$

$$U_{LH} = \frac{1}{2}\left(\frac{u_{BA3} + u_{S1}}{2} - \frac{u_{BA1} + u_{S3}}{2}\right), \tag{34}$$

$$\frac{\Delta u}{\Delta\theta_-} = \frac{1}{2}\left(\frac{u_{S3} - u_{BA2}}{\theta_{LH} - \theta_{\min}} + \frac{u_{BA1} - u_{S2}}{\theta_{LH} - \theta_{\min}}\right). \tag{35}$$

5.3. Calculation of control strategy parameters

5.3.1. Phase 3—Calculation of basic set of controller parameters

The basic set of PID controller parameters (for the region $\theta > \theta_{LH}$) is calculated according to Eqs. (10)–(13).

5.3.2. Phase 5—Calculation of other control strategy parameters

The optimal PID controller parameters for the region below the LH position ($\theta < \theta_{LH}$) are calculated by using Eqs. (14)–(16) from the basic set of controller parameters (Phase 3) and the estimated slope of the process static curve below the LH position, $\Delta u/\Delta\theta_-$. The parameter θ_{LH} of the control strategy (Fig. 6) is set to the LH position value estimated in phase 0. The parameters U_{Sc} and U_{LHc} of the nonlinear friction and LH compensators are calculated based on Eq. (18) and estimated values of friction voltage U_S and LH voltage U_{LH}.

5.4. Experimental verification of tuned control strategy

In order to test the tuned control strategy, the auto-tuning procedure was extended with an interval of control strategy verification. The control system response during this interval is shown in Fig. 15. The control system step response has the desired aperiodic form for all the tested operating modes, and the settling time is approximately 70 ms. The estimated parameters were found to agree well with the results of off-line identification (see e.g. Fig. 14). It should be noted that numerous auto-tuning experiments have been executed, and the estimated process parameters have always taken on similar values. This points out to the robustness of the auto-tuning strategy.

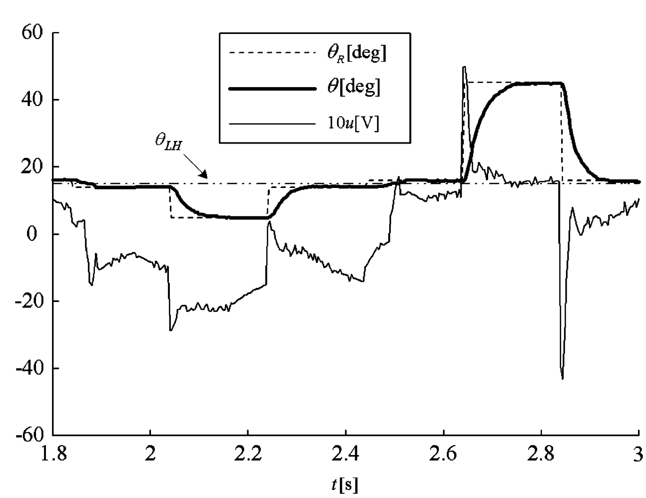

Fig. 15. Experimental response of electronic throttle control system tuned by auto-tuner.

6. Self-tuning of control strategy

In order to deal with the variations of battery voltage, armature resistance, and the LH position, which can occur within a single engine run, the control strategy is extended with a self-tuning procedure. It performs on-line estimation of process parameters and on-line calculation of the control strategy parameters.

6.1. Adaptation to variations of battery voltage

Since the battery voltage U_{bat} is measured in production vehicles, and K_{ch} is proportional to the battery voltage U_{bat}, its variations can be compensated for by scaling the controller output u (cf. Fig. 4):

$$u^* = uU_{bat0}/U_{bat}, \tag{36}$$

where U_{bat0} and U_{bat} represent nominal (initial) battery voltage and measured battery voltage, respectively.

6.2. Adaptation to armature resistance variations

The optimal parameters of the friction and LH compensators U_{LHc} and U_{Sc} for any value of armature resistance R_a are calculated according to Eqs. (18)–(20), provided that the initial values of process static curve parameters U_{LH0} and U_{S0} are known, and that the relative armature resistance R_a/R_{a0} can be estimated on-line. The initial values U_{LH0} and U_{S0} are obtained by the control strategy auto-tuning (Section 5). If the auto-tuner would not be executed, only partial adaptation of the nonlinear control strategy is carried out.

6.2.1. Direct estimation of R_a/R_{a0}

If the armature current measurement is available, the armature resistance can easily be estimated as the ratio of mean armature voltage and mean armature current for the throttle at standstill ($\omega_m \approx 0$; Fig. 4)

$$\hat{R}_a = \left.\frac{\bar{u}_a}{\bar{i}_a}\right|_{\omega_m\approx 0} = \left.\frac{K_{ch}\bar{u}}{\bar{i}_a}\right|_{\omega_m\approx 0}. \tag{37}$$

Mean values are used to suppress the noise in the current and voltage signals i_a and u.

The block diagram of the proposed self-tuning strategy is shown in Fig. 16. The standstill condition $\omega_m \approx 0$ is checked by monitoring the throttle speed signal ω (already available from the PID controller derivative term), with throttle zero speed threshold $\Delta_{\omega 0}$ set to double value of speed measurement resolution Δ_ω. Additional conditions on armature resistance estimation are (i) the mean armature current is not close to zero (to avoid division by zero in Eq. (37)), and (ii) the throttle is outside the highly nonlinear LH region ($|\theta - \theta_{LH}| > \varepsilon_{LH}$).

The estimated signal $\hat{R}_a/R_{a0}$ will include some noise and even possible spikes due to the noise in the estimator input signals i_a and u, and "non-ideal" enable logic. In order to suppress this noise, the estimated signal $\hat{R}_a/R_{a0}$ is filtered by a unit-gain low-pass filter (Fig. 16), whose bandwidth is chosen empirically to approximately 0.2 rad/s as a trade-off between fast estimation and low noise sensitivity.

6.2.2. Indirect estimation of R_a/R_{a0}

Simulation and experimental results in Deur et al. (2004) have shown that the steady-state point of the closed-loop control system falls on the middle curve of the hysteretic process static characteristic (so-called zero-friction curve, dotted curve in Fig. 5):

$$|u_{ss\pm}| = U_{LH\pm} + \frac{\Delta u}{\Delta\theta_\pm}|\theta - \theta_{LH}|. \tag{38}$$

Since the process static curve is proportional to the armature resistance (Eqs. (19) and (20)), the steady-state controller output is rewritten as

$$|u_{ss\pm}| = \frac{R_a}{R_{a0}}\left(U_{LH0\pm} + \frac{\Delta u}{\Delta\theta_{0\pm}}|\theta - \theta_{LH}|\right) = \frac{R_a}{R_{a0}}|u_{ss0\pm}|, \tag{39}$$

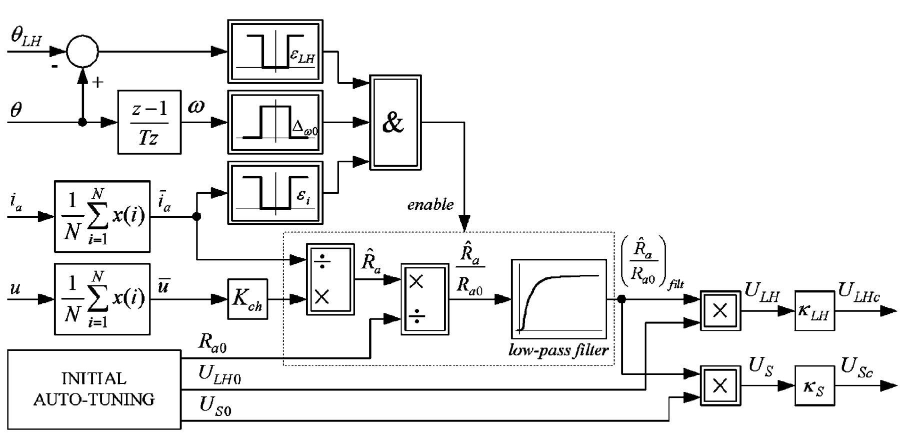

Fig. 16. Block diagram of self-tuning to armature resistance variations with available armature current measurement.

where $|u_{ss0\pm}|$ is the steady-state controller output calculated from initial process parameters $U_{LH0\pm}$ and $\Delta u/\Delta\theta_{0\pm}$.

According to Eq. (39), the ratio R_a/R_{a0} can be indirectly estimated as

$$\frac{R_a}{R_{a0}} = \frac{|u_{ss\pm}|}{|u_{ss0\pm}|}. \tag{40}$$

The block diagram of the proposed self-tuning law is shown in Fig. 17a. The steady-state controller output for initial process parameters, $|u_{ss0\pm}|$, is calculated according to Eq. (39). The switch SW in Fig. 17a transfers the ratio $|u|/|u_{ss0+}|$ if $\theta > \theta_{LH}$, or $|u|/|u_{ss0-}|$ if $\theta < \theta_{LH}$ to the smoothing low-pass filter whose output represents the estimated ratio $|u_{ss\pm}|/|u_{ss0\pm}|$. The filtering is enabled if the control error ε is small (the quasi-steady-state condition, $|\varepsilon| < \Delta_\varepsilon$), and if the throttle position θ and the throttle position reference θ_R are outside the highly nonlinear LH region. The threshold parameter Δ_ε is typically set to double value of position measurement resolution Δ_θ.

6.2.3. Estimation of LH voltage U_{LH} only

If the initial auto-tuning procedure is not available, only the LH voltage U_{LH} can be estimated. The expression for the LH voltage, given by Eq. (38), can be simplified to

$$U_{LH\pm} \approx |u_{ss\pm}|, \quad \text{if } |u_{ss\pm}| \gg \frac{\Delta u}{\Delta\theta_\pm}|\theta - \theta_{LH}|, \quad \forall\theta. \tag{41}$$

According to Section 2, the condition on $|u_{ss\pm}|$ in Eq. (41) is not satisfied well in the region $\theta < \theta_{LH}$ due to the return spring influence. Since this may introduce substantial overestimation of the LH voltage for $\theta < \theta_{LH}$, it would result in the LH overcompensation effect. In order to avoid the overcompensation effect, it is recommended that the LH correction factor κ_{LH} used in Eq. (18) is decreased for $\theta < \theta_{LH}$.

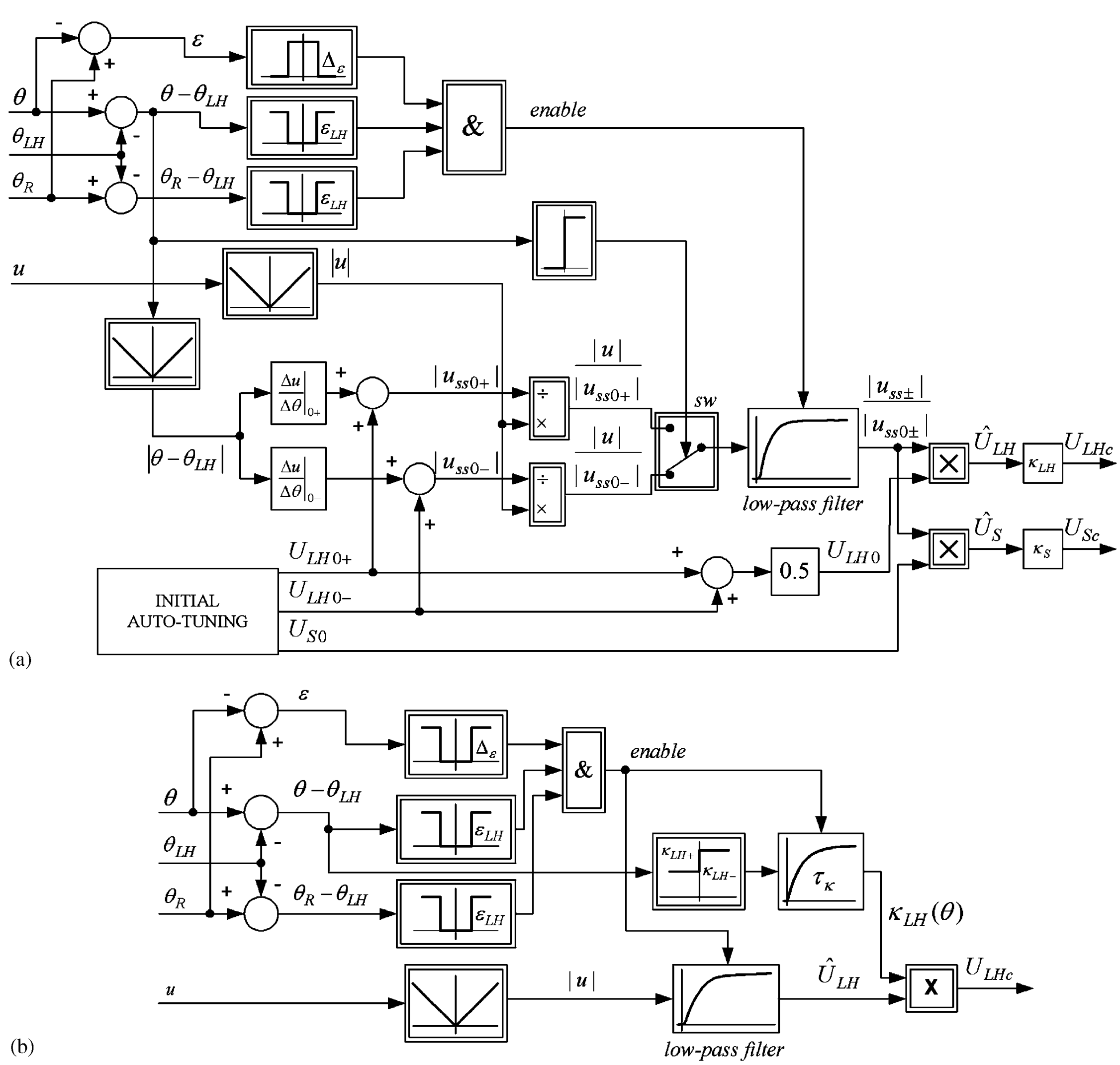

Fig. 17. Block diagrams of self-tuning to armature resistance variations without armature current measurement: with initial auto-tuning (a) and without initial auto-tuning (b).

The block diagram of the proposed self-tuning strategy with respect to LH voltage variations only is shown in Fig. 17b. The LH voltage is estimated as the filtered absolute value of the controller output (cf. Eq. (41)), where a low-pass filter is applied to suppress the noise in the estimated signal. The enable logic is the same as with the adaptive scheme in Fig. 17a. The correction factor κ_{LH} is modified by utilizing a lag term with the relay input, with correction factors $\kappa_{LH\pm}$ chosen empirically (Pavković & Deur, 2002).

6.3. Adaptation to LH position variations

The analysis in Section 4.3 may suggest that the negative influences of LH position variations could be avoided by widening the LH threshold ε_{LH}. However, in this way the friction compensator would be disabled in a relatively wide region around the assumed LH position (cf. Fig. 6), thus resulting in poor friction compensation performance in the region $\theta_{LH} \pm \varepsilon_{LH}$ (Pavković & Deur, 2002). Therefore, an adaptation algorithm based on on-line LH position estimation is proposed below.

The block diagram of an on-line LH position estimator is shown in Fig. 18. The estimation is enabled if the throttle is stuck ($|\bar{\omega}| < \Delta_{\omega 0}$) in the anticipated LH region ($|\theta - \theta_{LH0}| < \Delta_{\theta LH}$), and if the model following error is larger than a threshold ($|\varepsilon_m| > \Delta_\varepsilon$). In order to avoid the overshoot effect illustrated in Fig. 11, and related false detection of the LH position, the enable logic is extended with the condition $\mathrm{sgn}(\theta_m - \theta) = \mathrm{sgn}(\theta_R - \theta_m)$, or $(\theta_R - \theta_m)(\theta_m - \theta) > 0$ (as implemented in Fig. 18). The threshold parameters of the LH position estimator are set to the following values: $\Delta_{\theta LH} \approx 5\Delta_\theta$, $\Delta_{\omega 0} = 0.1\Delta_\omega$, and $\Delta_\varepsilon \leqslant 2U_{LH}T_I/(NTK_R)$ (see Pavković, 2003).

If all of the above conditions are satisfied, the *enable* signal in Fig. 18 is in the high state, and the current throttle position is held as the LH position θ_{LH} (sample & hold block in Fig. 18). This value is filtered in order to obtain bump-less adaptation of the control strategy.

6.4. Real-time simulation of process parameter variations

In order to provide verification of the proposed self-tuning control scheme, a real-time simulator of process parameters variations has been developed (Fig. 19). The simulator of armature resistance variations $\Delta u(\Delta R_a/R_{a0})$ is based on the motor armature model included in Fig. 4 (Pavković, 2003). Since the armature resistance change ΔR_a is supposed to be relatively slow, it is simulated as the step response of a low-pass filter. The simulator of LH position variations is implemented by presetting the false LH position data $\theta^*_{LH} \neq \theta_{LH}$ to the control strategy (see Fig. 19, and Pavković, 2003).

6.5. Experimental verification of self-tuning strategy

In all of the experiments, a random low-amplitude throttle reference changing around the LH position is used as a kind of a worst-case reference shape (see Fig. 20a). The randomized reference is implemented in a

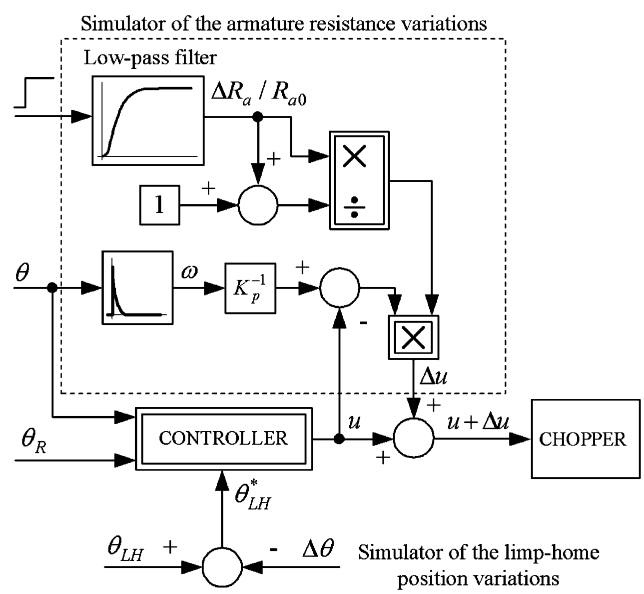

Fig. 19. Real-time simulator of process parameters variations.

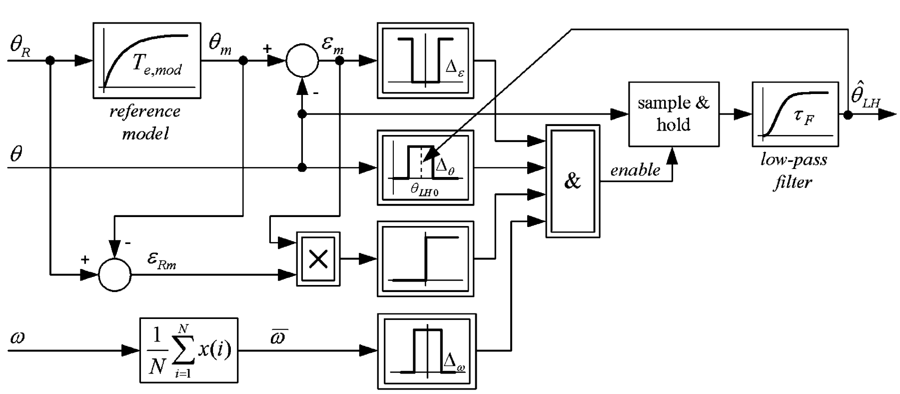

Fig. 18. Block diagram of self-tuning strategy with respect to variations of LH position.

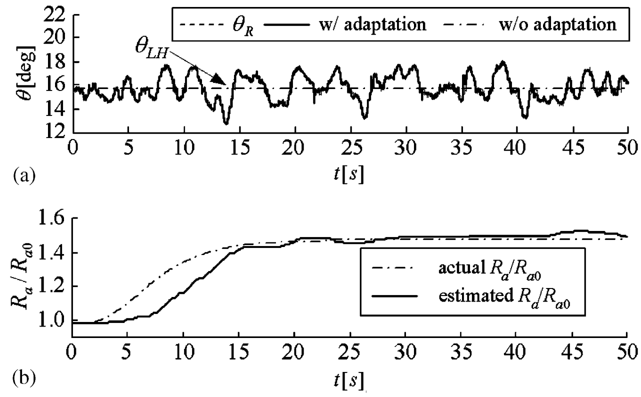

Fig. 20. Control system responses (a) and estimator response (b) for direct estimation of R_a/R_{a0}.

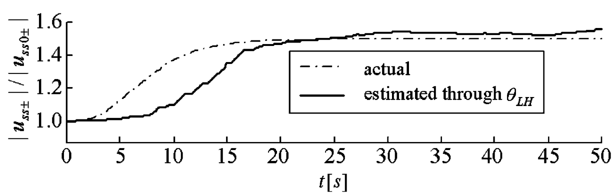

Fig. 21. Estimator response for indirect estimation of R_a/R_{a0}.

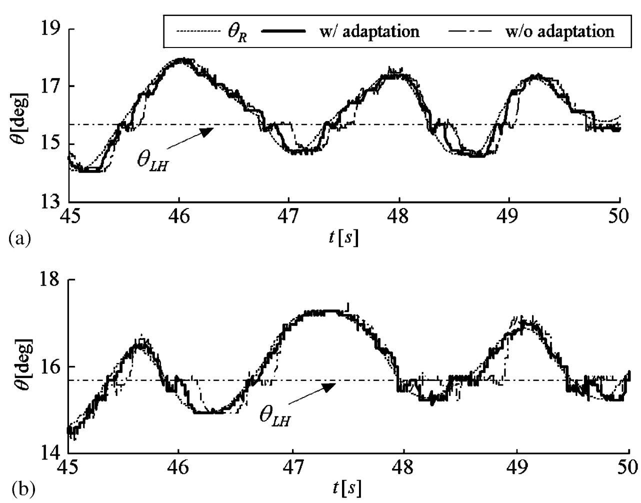

Fig. 22. Details of the throttle position responses for direct (a) and indirect (b) estimation of R_a/R_{a0}.

form of the low-pass filtered band limited white noise with a constant offset (Pavković, 2003).

The experimental results shown in Figs. 20–24 illustrate the effectiveness of the proposed self-tuning schemes. The direct estimation of armature resistance (Fig. 20) is accurate, with relatively small ripple in the steady-state response. The response (estimation) delay of approximately 5 s is caused by the narrow bandwidth of the applied low-pass filter, needed to reduce the ripple

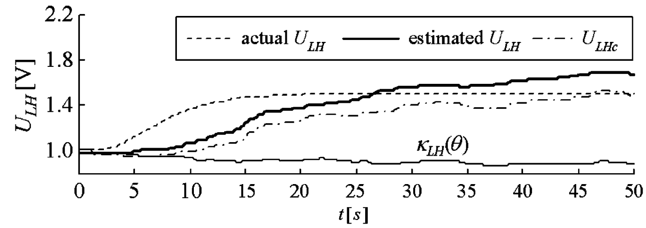

Fig. 23. Estimation of LH voltage only.

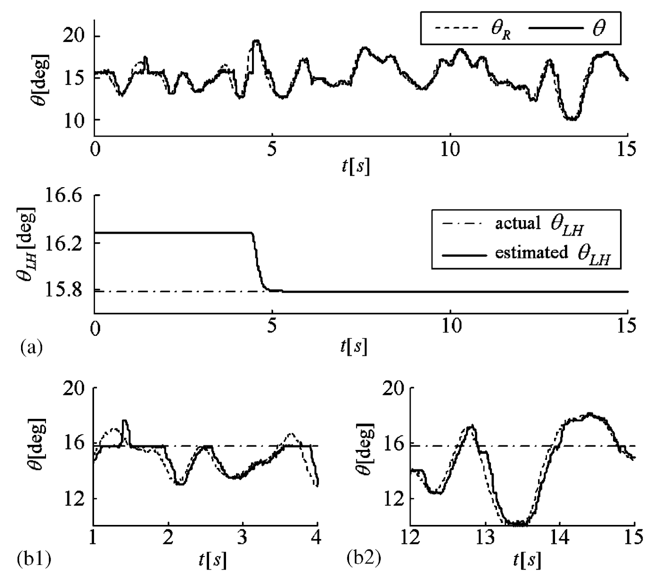

Fig. 24. Estimation of θ_{LH} (a), and detail of throttle position response before (b1) and after θ_{LH} is captured (b2).

in the estimated relative armature resistance R_a/R_{a0}. This delay is not emphasized when compared to relatively large delays of throttle temperature transients that cause the armature resistance change. The indirect estimation of armature resistance is also accurate (Fig. 21), but it is somewhat slower due to narrower bandwidth of the low-pass filter. The details of throttle position responses for direct (Fig. 22a) and indirect estimation (Fig. 22b) illustrate that the application of the adaptive control strategy significantly reduces the tracking error caused by the LH and stiction influences.

Fig. 23 shows the experimental results for the estimation of LH voltage U_{LH} only. The response of estimated LH voltage U_{LH} is characterized by a relatively large steady-state estimation error (overestimation). The error is compensated for in the estimator output signal U_{LHc} by applying a variable compensation correction factor $\kappa_{LH}(\theta)$.

The experimental responses for the estimation of LH position variations are shown in Fig. 24. The estimator of LH position variations correctly captures the actual value of LH position (Fig. 24a). The delay of the estimator response is caused by a conservative choice of

the model following error threshold Δ_ε, which is needed to provide robust estimation. The comparative response details in Fig. 24b clearly indicate the benefits of the application of LH adaptation: the adaptation results in significant reduction of the LH standstill intervals and throttle position overshoots.

7. Conclusion

A nonlinear strategy of electronic throttle control has been presented. The strategy includes linear feedback and feedforward controllers, and nonlinear friction and LH compensators. The presented experimental results have shown efficient rejection of the friction and LH effects that resulted in fast and accurate control system responses for the whole electronic throttle operating region.

A simulation analysis has been carried out in order to investigate the influence of process parameter variations on the behavior of the electronic throttle control system. The battery voltage and armature resistance variations result in proportional variations of the different process static curve voltage parameters, which, in turn, significantly affect the behavior of the nonlinear part of control system. On the other hand, the linear part of the electronic throttle control system is robust to the armature resistance and battery voltage variations. The analysis of the robustness with respect to LH position variations has pointed out to significant deterioration of the control system performance if the LH position varies outside the LH compensator activation threshold.

In order to improve the control system robustness, the control strategy has been extended with an adaptation mechanism consisting of auto-tuning and self-tuning algorithms. The auto-tuner application provides that all electronic throttles from a vehicle production series have similar (desired) control performance, regardless of variations of electronic throttle body parameters due to production deviations, external conditions variations, and aging. The auto-tuner does not require any prior knowledge of the process parameters. It is characterized by simple implementation and short execution time (about 1.5 s).

The self-tuning strategy has been developed in order to deal with process parameter variations which occur during a single engine run (i.e. those that cannot be captured by occasional utilization of the auto-tuner). These parameters are the battery voltage, the armature resistance, and the LH position. Since the battery voltage is measured in production vehicles, the self-tuning adaptation to battery voltage variations can be readily done by means of a gain-scheduling algorithm. The other two parameters, the armature resistance and the LH position, are estimated on-line based only on the standard electronic throttle measurement signals. The self-tuning strategy has been experimentally verified for the critical case of slow and stochastic changes of the reference throttle position through the LH region. The experimental results have demonstrated fast and accurate process parameter estimation, and consequently superior performance of the adaptive control strategy compared to the classical, non-adaptive strategy.

Acknowledgement

This work has been supported by Ford Motor Company and the Ministry of Science and Technology of the Republic of Croatia.

Appendix. On the block diagram formulation

Single-box blocks show step responses of linear terms. Two examples are given below.

Proportional term

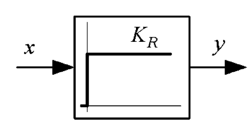

$y = K_R x$

First-order lag term

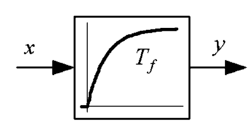

$T_f \dfrac{dy}{dt} + y = x$

Double-box blocks correspond to input–output maps of nonlinear terms. These are some examples:

Sign of x (times constant)

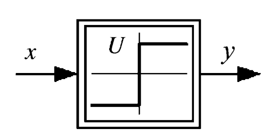

$y = U\,\mathrm{sgn}(x)$

Switching logic

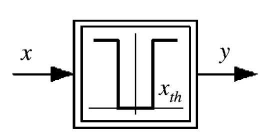

$y = \begin{cases} 0, & |x| < x_{th} \\ 1, & \text{otherwise} \end{cases}$

Look-up table

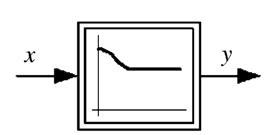

$y = f(x)$

Other blocks used are for basic arithmetic operations: $+, -, \times, \div$.

References

Barić, M., Petrović. I., & Perić, N. (2002). Neural network based sliding mode controller for a class of linear systems with unmatched uncertainties. *Proceedings of the 41st IEEE conference on decision and control (CDC'02)* (pp. 967–972). Las Vegas, Nevada, USA.

Barić, M., Petrović. I., & Perić, N. (2004). Neural network based sliding mode control of electronic throttle. *Proceedings of IFAC symposium on advances in automotive control*. Salerno, Italy.

Deur, J. (2001). Design of linear servosystems using practical optima. *Internal memorandum 04/19/01*, University of Zagreb, Croatia (translation of Chapter 3 of Ph.D. thesis by J. Deur).

Deur, J., & Pavković, D. (2002). Automatic tuning of electronic throttle control strategy. *Internal memorandum 06/15/02*, University of Zagreb, Croatia.

Deur, J., Pavković, D., Perić, N., Jansz, M., & Hrovat, D. (2004). An electronic throttle control strategy including compensation of friction and Limp–Home effects. *IEEE Transactions on Industry Applications*, *40*(3), 821–834.

Gagner, J., & Bondesson, R. (2000). *Adaptive realtime control of a nonlinear throttle unit*. Master's thesis, Department of Automatic Control, Lund Institute of Technology.

Hashimoto, E., Ishiguro, T., Yasui, Y., & Akazaki, S. (2003). Highly reliable electronic throttle system design. *SAE paper # 2003-01-0708*.

Huber, W., Lieberoth-Leden, B., Maisch, W., & Reppich, A. (1991). Electronic throttle control. *SAE Automotive Engineering*, *99*(6), 15–18.

Naslin, P. (1968). *Essentials of optimal control*. London: Iliffe Books Ltd (Chapter 2).

Pavković, D. (2003). *Identification and control of electronic throttle drive*. Master's thesis, Faculty of Electrical Engineering and Computing, University of Zagreb, Croatia.

Pavković, D., & Deur, J. (2002). Self-tuning control of an electronic throttle. *Internal memorandum 11/05/02*, University of Zagreb, Croatia.

Pavković, D., Deur, J., Jansz, M., & Perić, N. (2003). Experimental identification of electronic throttle body. *CD-ROM proceedings of 10th European conference on power electronics and applications (EPE 2003)*, Toulouse, France.

Rossi, C., Tilli, A., & Tonielli, A. (2000). Robust control of a throttle body for drive by wire operation of automotive engines. *IEEE Transactions on Control System Technology*, *8*(6), 993–1002.

Scattolini, R., Siviero, C., Mazzucco, M., Ricci, S., Poggio, L., & Rossi, C. (1997). Modeling and identification of an electromechanical internal combustion engine throttle body. *Control Engineering Practice*, *5*(9), 1253–1259.

Yokoyama, M., Shimizu, K., & Okamoto, N. (1998). Application of sliding-mode servo controllers to electronic throttle control. *Proceedings of the 37th IEEE conference on decision and control* (pp. 1541–1545). Tampa, Florida, USA.

Zäh, M., & Brandenburg, G. (1987). The extended damping optimum (in German). *Automatisierungstechnik*, *7*, 275–283.